Design Studies and Intelligence Engineering
L.C. Jain et al. (Eds.)

doi:10.3233/FAIA220728

Unsupervised Defect Detection for Medical Syringe Using Denoising Convolutional Autoencoder

Pengtao Wu [a], Xiaodong Wang [a,1], Fei Yan [a], and Zhiqiang Zeng [a]
[a] *College of Computer and Information Engineering, Xiamen University of Technology, Xiamen, China*

Abstract. Scale defect detection is an essential part of the quality control in the production process of medical syringes. Due to difficulty of collecting sufficient abnormal samples and defect types, it is impractical to optimize the deep learning model in a supervised learning manner for the defect detection of medical syringes. In this paper, we proposed an unsupervised defect detection method for medical syringes based on denoising convolutional autoencoder (DCAE). DCAE works as a deep reconstruction model, with a larger number of defect-free samples, to repair defects on anomaly samples reliably. The defects can be detected and located in the inspection phase by calculating the residual between the original and reconstructed images. The experimental results indicate that the proposed method is robust and can detect several scale defects in medical syringes. Our method reaches 95.11% average accuracy on one real-world medical syringe dataset, showing its practicality for defect detection.

Keywords. defect detection, medical syringe, unsupervised learning, denoising convolutional autoencoder

1. Introduction

After injection molding of medical syringes, the scale needs to be printed on its surface. The correct scale can help healthcare professionals control the dose of medication. On the contrary, incorrect scales could pose risks for the use of medical syringes and even cause medical malpractice. To ensure correct scales and prevent defective medical syringes from entering the market, we need to detect scale defects in the production phase of medical syringes. Figure 1 shows some samples of medial syringes containing incorrect scales. Since these abnormal scales are not significantly different from normal scales, it is difficult for operators who are prone to visual fatigue to provide reliable inspection results.

In recent years, benefiting from the rapid development of machine vision technology, various defect-detection techniques have shown promising results in the industrial field [1–3]. However, addressing the defect detection problem of medical syringes involves a few challenges in practice. In the first place, image processing techniques such as template matching are not competent for medical syringes' defect detection. In the actual production line, affected by various factors, the medical syringe images captured by

[1] Corresponding Author: Xiaodong Wang, E-mail: xdwangjsj@xmut.edu.cn

industrial cameras often present different brightness, contrast, and rotation angles. It is challenging to design a universal template to cover all the situations mentioned above. Next, the incidence of medical syringe defects is low, which led to insufficient collection of abnormal samples and imbalanced dataset. The factors mentioned above make the supervised machine learning framework not suitable for defect detection of medical syringes.

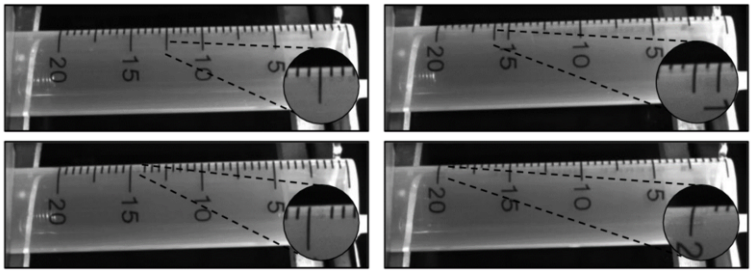

Figure 1. The anomalous samples of the medical syringe containing scale defects that looks like normal.

Instead of focusing on anomalous samples, some unsupervised techniques utilize enough normal data to build anomaly detectors, such as gaussian mixture model (GMM), generative adversarial network (GAN) [4], and autoencoder (AE) [5]. Autoencoder is a dimension reduction algorithm that has the ability for efficient representation learning of input data without any labels. Typically, the autoencoder is trained as a deep reconstruction model, using a large amount of normal data. This model is able to reconstruct the original data from the corrupted input data (anomalous data), and resultantly anomalies can be simply identified with a decision threshold. With the powerful representation capabilities of deep neural networks [6], convolutional neural network-based autoencoder (convolutional autoencoder) and their variants have been widely employed in the field of image anomaly detection. For instance, Chow et al. [7] applied a convolutional autoencoder (CAE) to anomaly defect detection of concrete structure. Kozamernik et al. [8] used the variational convolutional autoencoder (VCAE) to detect anomalies on KTL coatings. Mei et al. [9] constructed a denoising convolutional autoencoder (DCAE) to complete the automatic defect detection system for textile fabric. In these studies, the autoencoder performs well in detecting abnormal samples even if only normal training samples are available.

Inspired by above studies, this paper attempts to address the problem of defect detection in medical syringes based on denoising convolutional autoencoder (DCAE), a variant of the convolutional autoencoder (CAE), with stronger feature encoding capabilities. First of all, in order to shorten the time of model design and verification, this article constructed a DCAE model based on SegNet [10]. Subsequently, sufficient defect-free samples were collected on the medical syringe production line for DCAE training. After DCAE adds specific noise to the training samples, it will learn how to reconstruct and repair these noise samples to encode the key features of medical syringes. When testing the model, DCAE can effectively repair the defects in abnormal samples. Finally, the image processing technique was applied to achieve the detection and localization of defects. Experimental results on one real-world dataset with several types of defects demonstrate that the proposed method can effectively and robustly detect and locate defects of medical syringes.

The remainder of this paper is organized as follows: Section 2 elaborates the proposed methodology. The results are analyzed and discussed in Section 3. Section 4 concludes this article with the summary and outlook for future work.

2. Methodology

In this section, we present a description of the proposed defect detection framework of medical syringes in detail. Figure 2 shows the overall architecture of this framework. In the training phase, defect-free samples are fed into DCAE for training and let DCAE encode key features of medical syringes for defect reconstruction. In the testing phase, DCAE will reconstruct and repair the input sample and then use image processing technique to identify scale defects.

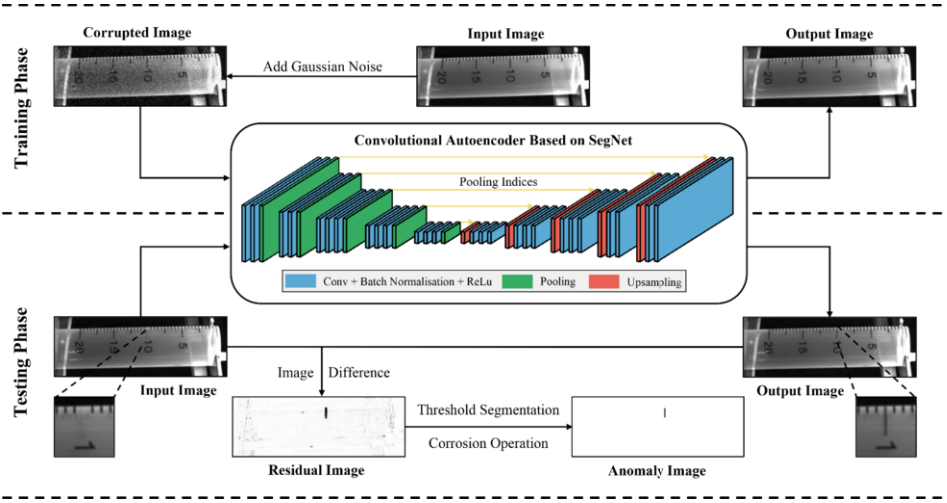

Figure 2. Overall architecture of the proposed DCAE model.

2.1. Network Architecture

CAEs are widely used as a base framework for image anomaly detection in an unsupervised manner. The goal of using CAEs is to train them to reconstruct normal samples as perfectly as possible. During testing, they attempt to reconstruct and repair the anomalous samples that were not involved in the training. And then, we can detect and locate anomalies by comparing the input and its reconstruction pixel-by-pixel.

The workflow of a typical CAE can be divided into two stages, namely encoding and decoding. The detailed process can be formulated as follows:

$$h = f(x), \tag{1}$$

$$\tilde{x} = g(h) = g(f(x)), \tag{2}$$

$$Loss = \left\| x - \tilde{x} \right\|_p . \tag{3}$$

The function $f(\cdot)$ in Equation 1 encodes input image x into a feature space h with lower dimensionality. Instead, the function $g(\cdot)$ in Equation 2 decodes the latent feature h to generate reconstructed image. The goal is to optimize $f(\cdot)$ and $g(\cdot)$ and minimize the loss function in Equation 3, where p is usually set to 1 (l_1-norm) or 2 (l_2-norm). To obtain robust feature encoding h, we can add specific noise to the input image x in the CAE's training phase, which is also called the DCAE [11]. The core idea of the DCAE is to learn the essential characteristics in repairing the damaged image to establish a more stable encoding in the hidden layer. In this paper, we add Gaussian noise with a mean of zero and a variance of 0.01 to input image x during the training.

For a reliable and effective defect detection, we propose to utilize the SegNet as our backbone network. SegNet is a deep fully convolutional neural network proposed by Badrinarayanan et al. [10] to solve the problem of image segmentation. It refers to the topology structure of the VGG16 [12] to construct the encoder and the decoder. The novelty of SegNet lies in its unique up-sampling operation, which can effectively reduce network parameters and improve network performance while retaining image characteristics. Due to the final output of SegNet is a probability map of the image pixels rather than a reconstructed image, which cannot be directly applied to the unsupervised defect detection application. Therefore, we directly remove the softmax layer of the SegNet and employ it as the DCAE's backbone network.

2.2. Loss Function

To train DCAE, we can directly deploy the Mean Squared Error (MSE) loss function. However, the l_2 distance in MSE evaluates the difference between the two images under the assumption that each pixel is independent of each other, which may cause the model to fail to capture the structural information of the image during the reconstruction process. As shown in Figure 1, the scale of the medical syringes has obvious structural information, that is, the black stripes of different lengths arranged in parallel. We try to make the model perceive this structural information of normal samples during the training process to repair and extract scale defects in abnormal samples more efficiently. Accordingly, we introduce the structural similarity (SSIM) index [13] into DCAE.

SSIM index evaluates the similarity of two images in terms of brightness, contrast, and structure. Compared with the traditional l_2-norm, it can perceive the structural differences between images. By incorporating the SSIM index into the loss function, the defect segmentation performance of the CAE can be significantly improved [14]. In practical applications, we usually adopt the SSIM index to evaluate the local similarity of images instead of global one. For the given two $n \times n$ local windows $\mathbf{x}$ and $\mathbf{y}$ (located at the same place) of the different images $\mathbf{X}$ and $\mathbf{Y}$, the calculation formula of SSIM index is as follows:

$$SSIM(\mathbf{x},\mathbf{y}) = \frac{(2\mu_x\mu_y + C_1)(2\sigma_{xy} + C_2)}{(\mu_x^2 + \mu_y^2 + C_1)(\sigma_x^2 + \sigma_y^2 + C_2)}, \tag{4}$$

where μ_x and μ_y represent the mean value of $\mathbf{x}$ and $\mathbf{y}$, respectively; σ_x^2 and σ_y^2 represent the variances of $\mathbf{x}$ and $\mathbf{y}$, respectively; σ_{xy} represents the covariance of $\mathbf{x}$ and $\mathbf{y}$; C_1 and C_2 are two constants to prevent division by zero.

For assessment of global structural similarity between two images, we can pass a sliding window pixel-by-pixel through the entire image to compute SSIM index of all local windows and generate SSIM index map [15]. Assuming $\mathbf{W}_{i,j}^x$ and $\mathbf{W}_{i,j}^y$ are the sliding windows at (i, j) of image $\mathbf{X}$ and $\mathbf{Y}$, respectively. the global average SSIM index (MSSIM index) of the image $\mathbf{X}$ and $\mathbf{Y}$ can be calculated as follows:

$$MSSIM(\mathbf{X},\mathbf{Y}) = \frac{1}{MN}\sum_{\forall i,j} SSIM(\mathbf{W}_{i,j}^x, \mathbf{W}_{i,j}^y), \tag{5}$$

where M and N denote the width and height of the image. In this article, we use a local window of size 11×11 to calculate the MSSIM index during the DCAE's training phase. A larger MSSIM value indicates that the two images are more similar. When the MSSIM value is 1, the two images are identical. Thus, we define our loss function as:

$$LOSS = 1 - MSSIM(\mathbf{X},\mathbf{Y}). \tag{6}$$

2.3. Detecting Defects

Combined with the above data augmentation technology and loss function, the model can be used to detect scale defects of the medical syringe after completing the training. Figure 2 briefly shows the primary process of defect detection, and the detailed procedure is as follows:

First, the medical syringe samples to be tested are fed into the defect detection model, and then the testing samples are restoratively reconstructed using the features already encoded by the model. To verify how well the testing samples are reconstructed, we evaluate the SSIM index between the testing and the reconstructed samples, and output the SSIM index map as a residual map. Let I^{tes} and I^{rec} be the testing image and reconstructed image, respectively. The residual map I_{res} can be formulated as follows:

$$I_{res}(i,j) = SSIM(\mathbf{W}_{i,j}^{tes}, \mathbf{W}_{i,j}^{rec}),\ s.t.\ \forall i,j, 1 \le i \le M, 1 \le j \le N, \tag{7}$$

where $\mathbf{W}_{i,j}^{tes}$ and $\mathbf{W}_{i,j}^{rec}$ denote the sliding window centered at location (i, j) in the image I^{tes} and I^{res}, respectively; It is worth noting that we use SSIM instead of pixel-by-pixel difference to output the residual map. This can effectively avoid the error segmentation caused by the excessive residual of individual pixels. In this stage, different from the training phase, we use a 3×3 sliding window size when outputting the SSIM index map to get a finer residual map.

The residual map can be considered as the reconstruction error of the model on the input image. Therefore, we can impose a threshold segmentation operation on the residual map to obtain an anomaly map. This process can be expressed as follows:

$$I_{ano}(i,j)=\begin{cases}255, & I_{res}(i,j)>T,\\ 0, & I_{res}(i,j)\le T,\end{cases} \tag{8}$$

where $I_{ano}(i,j)$ denotes the pixel value of the anomaly map at location (i,j), T is the segmentation threshold. The pixel values of 0 and 255 represent abnormal and normal pixels, respectively. After threshold segmentation, we applied the corrosion operation to eliminate some subtle mis-segmentations in the abnormal map. By judging whether there are abnormal pixels in the abnormal map, anomalous images can be distinguished from the test images. For the segmentation threshold T, we determined it on the validation set after completing model training. To be specific, we traverse all segmentation thresholds (0~255) to evaluate the F1-Measure of the model on the validation set. The threshold corresponding to the highest F1-Measure will be selected as the optimal threshold T for model testing.

3. Experiments

3.1. Dataset and Augmentation

The dataset used in this paper was collected from the actual production line of medical syringes. This dataset consists of 1,200 defect-free images, all of which are single-channel grayscale images captured by industrial cameras. Figure 3 illustrates some examples of images in the dataset, including medical syringes with different placement and rotation angles. The entire dataset was split into (training set, validation set, and test set) with the ratio of 6:2:2, and we finally obtained 720 training images, 240 validation images, and 240 test images.

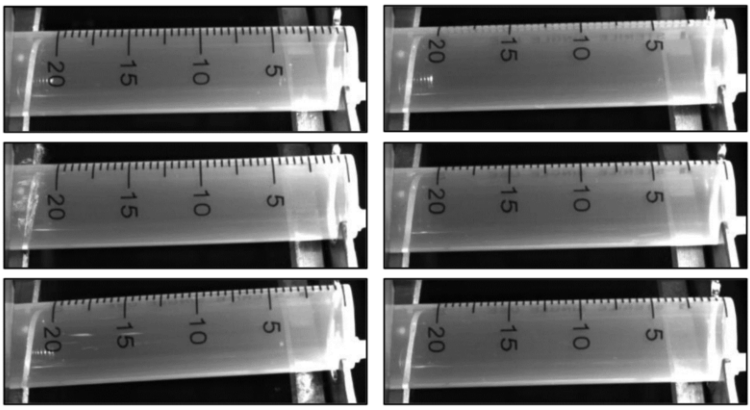

Figure 3. Medical syringe samples without any scale defects.

Similar to existing deep neural networks, our DCAE maintains a numerous number of parameters and requires an enormous amount of training data to guarantee that the network could pursue the accurate feature extraction [16]. Furthermore, the medical syringe images captured in the industrial production process often exhibit different brightness, contrast, and rotation angles. It is hard to collect sufficient training samples

covering all these factors. Therefore, if we simply use the images in our dataset for training, the model will be at risk of low performance and poor generalization. To get rid of this problem, we expand the dataset using the following approaches:

- Randomly select a brightness factor from [50%,60%,70%,· · ·,140%,150%] to adjust the brightness for each image.
- Randomly select a contrast factor [50%,60%,70%,· · ·,140%,150%] to adjust the contrast for each image.
- Rotate each image with a degree that is randomly selected from {-5,-4,· · ·,4,5}.

We use the above three data augmentation methods to expand 720 training images and get 2,160 enhanced images (each method expands 720 images). In total, we obtain 2,880 non-defect training images as training set.

The abnormal samples on the production line of medical syringes are scarce, which is not enough to validate and test the performance of the model. To solve this problem, we construct validation and test sets by making artificial scale defects on the validation and test images, respectively.

In the CAE system, a decision threshold is usually required to determine whether each pixel of the input image is anomalous or not. In this article, we intend to determine this threshold on the validation set. Considering that scale defects during the production of medical syringes are often variable and unpredictable, we utilize the "Random Erasing" method to produce artificial defects on validation images. In other words, the reason for generating defects in this random way is that we want to obtain a decision threshold that is suitable for the majority of scale defects, so as to improve the generalization of the model. For the test set, we refer to the existing abnormal samples (as shown in Figure 1) and carefully craft two types of scale defects on 240 defect-free test images. Finally, we obtained one validation set and two test sets with different scale defects. Each test set contains 240 defect images and 240 defect-free images. Figure 4 shows these artificial scale defects in detail, where Figures 4(a), 4(b), and 4(c) represent random scale defects on the validation set, scale error defects and scale missing defects on the test set, respectively.

The original size of all images in our dataset is 1050×360 pixels, and these images will be scaled to 350×120 pixels for model training and testing.

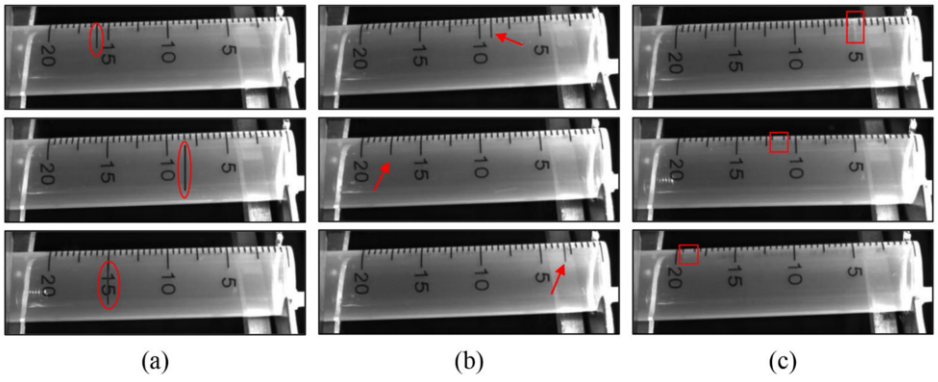

Figure 4. Examples of artificial defects, where Figures 4(a), 4(b), and 4(c) represent random scale defects, scale error defects, and scale missing defects, respectively.

3.2. Experimental Setting

Training Setting: We optimized model parameters using the Adam algorithm [17] and set the initial learning rate as 0.001. The model was implemented in Pytorch and trained for 300 epochs with a batch size of 16 on an NVIDIA GeForce GTX 2080 Ti GPU.
Evaluation Criteria: The defect detection model proposed in this paper is used to judge whether a medical syringe image contains defects or not, which can be regarded as a binary classification problem. In the model evaluation phase, we define medical syringe images containing defects as positive samples (abnormal samples) and normal medical syringe images as negative samples (normal samples). We introduce four classifier metrics to evaluate model performance, including accuracy, precision, recall, and F1-Measure. These metrics are formulated as follows:

$$Accuracy = \frac{TP + TN}{TP + TN + FP + FN}, \tag{9}$$

$$Precision = \frac{TP}{TP + FP}, \tag{10}$$

$$Recall = \frac{TP}{TP + FN}, \tag{11}$$

$$F1 - Measure = \frac{2 \times Precision \times Recall}{Precision + Recall}, \tag{12}$$

where TP and TN represent the numbers of correctly classified positive and negative samples, respectively; FP and FN represent the number of positive and negative samples that are miss-classified.

3.3. Model Performance

In Figure 5, we show the defect detection results obtained by DCAE for two typical scale defects in detail. Overall, DCAE is able to reconstruct and repair defective areas almost completely for most anomalous samples. Thanks to the excellent abnormal reconstruction capabilities, some tiny scale defects also can be accurately located, e.g, the defects in Figure 5(c),(g). Moreover, it can be seen from this figure that DCAE has good adaptability to medical syringes with different rotation angles. Even though some samples have large angular deviations, DCAE still reconstructs them well and segments the defects, e.g, the samples in Figure 5(b),(f).

Table 1 presents the classification performance of DCAE on our medical syringe dataset. In the detection of different kinds of scale defects, the average accuracy, precision, recall and F1-Measure of this model reach 95.11%, 96.46%, 93.91%, and 95.15%, respectively. This indicates that our model has good anomaly detection capability, which can effectively prevent defect samples from missing inspection and can meet the demand of enterprises. We can also observe that the anomaly detection ability of our model for scale error defects is better than that of scale missing defects. The reason may lie in that there are more structural information reduction in the scale missing defects

than that of the scale error defects. As shown in Figure 5(d), we can see that the scale missing defect is quite subtle and is even hard for human to notice it, posing a great challenge for defect detection models. The repaired scale is shown in a lighter color in the bottom line, which is somewhat different from the original scale of the medical syringe, resulting a failure in defect detection. The detection results for the scale error defects are shown in Figure 5(a)-(c). We can find out that our model repairs the scale error defects nearly perfectly, e.g, the sample in Figure 5(a), demonstrating that our model can meet the demand of real-world medical syringe defect detection.

To verify that our transformation work is necessary and effective, we also constructed a convolutional autoencoder (CAE) model for defect detection based on SegNet. CAE uses the same network architecture as DCAE, except that it does not add specific noise to the input samples during the training process. In addition, we used MSE as the loss function to optimize DCAE, namely DCAE+MSE, to further confirm the advantages of the SSIM index. Subsequently, we evaluated the performance of two new models on scale missing and scale error test sets. The average classification performance of different models on our medial syringe dataset is presented in Table 2. Regardless of which model is employed, the defect detection performance of SSIM loss function is significantly better than that of MSE. This may be credited to the structural characteristics of SSIM loss, which can preserve the scale features of medical syringe while reconstructing, thereby improving the model's reconstruction ability and prediction performance. Additionally, it can be seen from Table 2 that compared with CAE, DCAE's architecture can also boost the defect detection performance. This is because that DCAE can establish more robust feature encoding in the process of reconstructing noisy samples. These stable feature encodings are beneficial for repairing defects in abnormal samples and further enhance the accurate rate of defect detection.

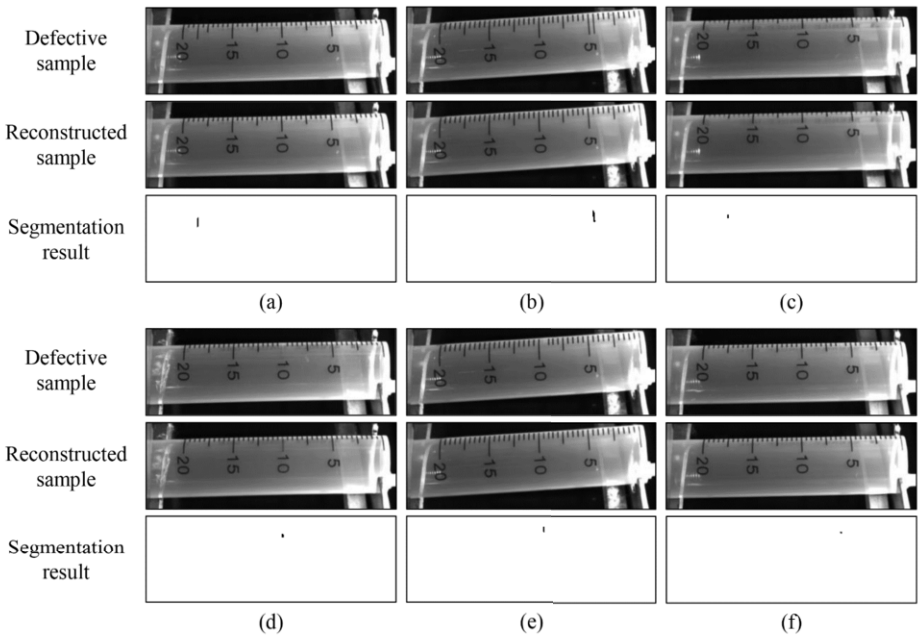

Figure 5. Defect detection results of scale error and scale missing images. Each group of images (top to bottom) contains the defective sample, the reconstructed image, and the segmentation result.

Table 1. Defect detection results for the proposed DCAE model.

Defect Type	Accuracy	Precision	Recall	F1-Measure
Scale Missing	93.54%	93.33%	93.72%	93.53%
Scale Error	96.67%	99.58%	94.09%	96.76%
All Types	95.11%	96.46%	93.91%	95.15%

Table 2. Performance comparison of different models on our medical syringe dataset.

Model	Accuracy	Precision	Recall	F1-Measure
CAE+SSIM	74.38 %	73.75%	79.31%	75.47%
DCAE+MSE	64.06%	89.38%	59.14%	71.13%
DCAE+SSIM	95.11%	96.46%	93.91%	95.15%

4. Conclusion and Future Work

From the perspective of unsupervised learning, this paper presented a defect detection model for medical syringes based on denoising convolutional autoencoder. After reconstructing a large number of defect-free images containing noise, our model establishes a more stable feature representation for medical syringes. After that, scale defects contained in abnormal samples can be repaired while testing, and can be subsequently detected via residual maps. This reconstruction-repair approach can efficiently detect abnormal samples when only normal samples are available. We evaluated the detection performance of our model for different scale defects on two test sets of medical syringes, and its average accuracy and F1-Measure reached 95.11% and 95.15%, respectively, effectively solving the defect detection problem of medical syringes.

Although our model achieves high-accuracy defect detection, its vast and complex network suffers from the problem of slow detection. In the future work, we will introduce the pruning algorithm [18] into the model to improve the detection efficiency.

5. Acknowledgments

This paper was supported by National Natural Science Foundation of China (Grant Nos. 61871464, U1805264), National Natural Science Foundation of Fujian Province (Grant Nos. 2021J011186, 2020J01266), the “Climbing” Program of XMUT (Grant No. XPDKT20031), Scientific Research Fund of Fujian Provincial Education Department (Grant No. JAT200486), the University Industry Research Fund of Xiamen (Grant No. 2022CXY0416).

References

[1] Y.G. Yoon, S.L. Lee, C.W. Chung, and S.H. Kim. An effective defect inspection system for polarized film images using image segmentation and template matching techniques. Computers & Industrial Engineering, 55(3):567–583, 2008.

[2] X. Zhang, Y. Ding, Y. Lv, A. Shi, and R. Liang. A vision inspection system for the surface defects of strongly reflected metal based on multi-class svm. Expert Systems with Applications, 38(5):5930–5939, 2011.

[3] L. Shang, Q. Yang, J. Wang, S. Li, and W. Lei. Detection of rail surface defects based on cnn image recognition and classification. In 2018 20th International Conference on Advanced Communication Technology (ICACT), pages 45–51. IEEE, 2018.
[4] Ian Goodfellow, Jean Pouget-Abadie, Mehdi Mirza, Bing Xu, David Warde-Farley, Sherjil Ozair, Aaron Courville, and Yoshua Bengio. Generative adversarial networks. Communications of the ACM, 63(11):139–144, 2020.
[5] G.E. Hinton and R.R. Salakhutdinov. Reducing the dimensionality of data with neural networks. science, 313(5786):504–507, 2006.
[6] Yi Yang, Yueting Zhuang, and Yunhe Pan. Multiple knowledge representation for big data artificial intelligence: framework, applications, and case studies. Frontiers of Information Technology & Electronic Engineering, 22(12):1551–1558, 2021.
[7] J.K. Chow, Z. Su, J. Wu, P.S. Tan, X. Mao, and Y.H. Wang. Anomaly detection of defects on concrete structures with the convolutional autoencoder. Advanced Engineering Informatics, 45:101105, 2020.
[8] N. Kozamernik and D. Bra˘cun. Visual inspection system for anomaly detection on ktl coatings using variational autoencoders. Procedia CIRP, 93:1558–1563, 2020.
[9] S. Mei, Y. Wang, and G. Wen. Automatic fabric defect detection with a multi-scale convolutional denoising autoencoder network model. Sensors, 18(4):1064, 2018.
[10] V. Badrinarayanan, A. Kendall, and R. Cipolla. Segnet: A deep convolutional encoder-decoder architecture for image segmentation. IEEE transactions on pattern analysis and machine intelligence, 39(12):2481–2495, 2017.
[11] P. Vincent, H. Larochelle, Y. Bengio, and P.A. Manzagol. Extracting and composing robust features with denoising autoencoders. In Proceedings of the 25th international conference on Machine learning, pages 1096–1103, 2008.
[12] K. Simonyan and A. Zisserman. Very deep convolutional networks for large-scale image recognition. arXiv preprint arXiv:1409.1556, 2014.
[13] Z. Wang, A.C. Bovik, and E.P. Simoncelli. Structural approaches to image quality assessment. Handbook of image and video processing, 7(18), 2005.
[14] P. Bergmann, S. L¨owe, M. Fauser, D. Sattlegger, and C. Steger. Improving unsupervised defect segmentation by applying structural similarity to autoencoders. arXiv preprint arXiv:1807.02011, 2018.
[15] Alireza Nasiri Avanaki. Exact global histogram specification optimized for structural similarity. Optical review, 16(6):613–621, 2009.
[16] A. Krizhevsky, I. Sutskever, and G.E. Hinton. Imagenet classification with deep convolutional neural networks. Advances in neural information processing systems, 25:1097–1105, 2012.
[17] D.P Kingma and J. Ba. Adam: A method for stochastic optimization. arXiv preprint arXiv:1412.6980, 2014.
[18] Xiaodong Wang, Zhedong Zheng, Yang He, Fei Yan, Zhiqiang Zeng, and Yi Yang. Soft person reidentification network pruning via blockwise adjacent filter decaying. IEEE Transactions on Cybernetics,2021.